Location of the Fluoride Ion in Tetrapropylammonium Fluoride Silicalite-1 Determined by $^{1}H/^{19}F/^{29}Si$ Triple Resonance CP, REDOR, and TEDOR NMR Experiments

Colin A. Fyfe,*,† Darren H. Brouwer,† Andrew R. Lewis,† and Jean-Michel Chézeau‡

Contribution from the Department of Chemistry, University of British Columbia, 2036 Main Mall, Vancouver BC, Canada V6T 1Z1, and Laboratoire de Matériaux Minéraux, UPRES-A 7016 CNRS, Ecole Nationale Supérieure de Chimie de Mulhouse, 3 rue Alfred Werner F-68093, Mulhouse Cedex, France

Received February 27, 2001. Revised Manuscript Received May 9, 2001

Abstract: The location of the fluoride ion in tetrapropylammonium fluoride silicalite-1 ([TPA]-F-[Si-MFI]), an as-synthesized siliceous zeolite with the MFI topology, has been unambiguously determined using solid-state NMR experiments alone. With the $^{1}H\rightarrow^{29}Si$ CP-INADEQUATE experiment, the 12 peaks in the highly resolved ^{29}Si MAS NMR spectrum of [TPA]-F-[Si-MFI] were assigned. Using these peak assignments it was possible to perform $^{1}H/^{19}F/^{29}Si$ triple resonance CP, REDOR, and TEDOR experiments to measure F−Si distances and thus locate the fluoride ion. It is covalently bonded to Si-9 in the $[4^{1}5^{2}6^{2}]$ cage of the zeolite framework and exchanges between two "mirror-related" Si-9 sites, making them equivalent on the NMR time scale. The importance of this result and the general applicability of the approach are discussed.

Introduction

Zeolites and related microporous materials are commonly prepared by hydrothermal crystallization of alkaline reaction mixtures. For highly siliceous materials, this synthetic route generally leads to substantial numbers of Q_3 Si−O^- and Si−OH defect sites which can be observed by ^{1}H and ^{29}Si magic angle spinning (MAS) NMR.[1] During the past 20 years, an alternate synthetic route has been developed that can be carried out near neutral pH and employs fluoride ions as the mineralizing agent rather than hydroxide ions, as first reported by Flanigen and Patton for the synthesis of fluoride silicalite-1.[2] In subsequent years, the scope of this synthesis route has been further extended by Guth, Kessler, and co-workers[3−6] and more recently by Camblor and co-workers.[7]

The most notable difference between the fluoride and hydroxide synthetic routes is that materials synthesized in fluoride media have been shown to have substantially fewer defect sites.[8,9] Another important aspect of the fluoride synthetic route is that larger crystals can be made[3,10] and it has also afforded pure silica phases with low framework densities.[7] In addition, the fluoride route can be used to prepare catalytically active materials by incorporating other elements such as B, Al, Fe, Ga, Ge, and Ti into the framework[3−5] and to prepare non-silicon-based microporous materials such as $AlPO_4$s and $GaPO_4$s.[6]

Because of the superior quality of the products, there is considerable interest in understanding the role that the fluoride ions play in the synthesis of zeolites under these conditions. The initial motivation for including fluoride ions in the synthesis mixture was for F^- to replace OH^- as the mineralizing agent since the solid silica sources are not soluble near neutral pH. It has also been proposed that the fluoride ions may catalyze the condensation reaction involved in Si−O−Si bond formation.[11] However, chemical analysis,[3,4] solid-state ^{19}F and ^{29}Si MAS NMR spectroscopy,[12−16] and X-ray diffraction (XRD) studies[17−20]

* Address correspondence to this author. E-mail: fyfe@chem.ubc.ca.
† University of British Columbia.
‡ Ecole Nationale Supérieure de Chimie de Mulhouse.

(1) Koller, H.; Lobo, R. F.; Burkett, S. L.; Davis, M. E. *J. Phys. Chem.* **1995**, *99*, 12588.
(2) Flanigen, E. M.; Patton, R. L. United States Patent No. 4073865, 1978.
(3) Guth, J. L.; Kessler, H.; Wey, R. In *New Developments in Zeolite Science and Technology, Proceedings of the 7th International Zeolite Conference*; Murakami, Y., Iijima, A., Ward, J. W., Eds.; Elsevier: Amsterdam, 1986; p 121.
(4) Guth, J. L.; Kessler, H.; Higel, J. M.; Lamblin, J. M.; Patarin, J.; Seive, A.; Chézeau, J. M.; Wey, R. *Am. Chem. Soc. Symp. Ser.* **1989**, *389*, 176.
(5) Guth, J. L.; Kessler, H.; Caullet, P.; Hazm, J.; Merrouche, A.; Patarin, J. In *Proceedings from the 9th International Zeolite Conference*; von Ballmoos, R., Higgins, J. B., Treacy, M. M. J., Eds.; Butterworth-Heinemann: Stoneham, MA, 1993; Vol. I, p 215.
(6) Kessler, H.; Patarin, J.; Schott-Darie, C. *Stud. Surf. Sci. Catal.* **1994**, *85*, 75.
(7) Camblor, M. A.; Villaescusa, L. A.; Díaz-Cabañas, M. J. *Top. Catal.* **1999**, *9*, 59.
(8) Chézeau, J. M.; Delmotte, L.; Guth, J. L.; Soulard, M. *Zeolites* **1989**, *9*, 78.
(9) Chézeau, J. M.; Delmotte, L.; Guth, J. L.; Gabelica, Z. *Zeolites* **1991**, *11*, 598.
(10) Kuperman, A.; Nadimi, S.; Oliver, S.; Ozin, G. A.; Garces, J. M.; Olken, M. M. *Nature* **1993**, *365*, 239.
(11) Barrett, P. A.; Camblor, M. A.; Corma, A.; Jones, R. H.; Villaescusa, L. A. *J. Phys. Chem. B* **1998**, *102*, 4147.
(12) Koller, H.; Wölker, A.; Villaescusa, L. A.; Díaz-Cabañas, M. J.; Valencia, S.; Camblor, M. A. *J. Am. Chem. Soc.* **1999**, *121*, 3368.
(13) Koller, H.; Wölker, A.; Eckert, H.; Panz, C.; Behrens, P. *Angew. Chem., Int. Ed. Engl.* **1997**, *36*, 2823.
(14) Marcuccilli Hoffner, F.; Delmotte, L.; Kessler, H. *Zeolites* **1993**, *13*, 60.
(15) Delmotte, L.; Soulard, M.; Guth, F.; Seive, A.; Lopez, A.; Guth, J. L. *Zeolites* **1990**, *10*, 778.
(16) Klock, E.; Delmotte, L.; Soulard, M.; Guth, J. L. In *Proceedings of the 9th International Zeolite Conference*; von Ballmoos, R., Higgins, J. B., Treacy, M. M. J., Eds.; Butterworth-Heinemann: Stoneham, MA, 1993; Vol. I, p 611.
(17) Caullet, P.; Guth, J. L.; Hazm, J.; Lamblin, J. M.; Gies, H. *Eur. J. Solid State Inorg. Chem.* **1991**, *28*, 345.
(18) van de Goor, G.; Freyhardt, C. C.; Behrens, P. *Z. Anorg. Allg. Chem.* **1995**, *621*, 311.

10.1021/ja010532v CCC: $20.00
Published on Web 06/20/2001

reveal that many of the as-synthesized zeolites incorporate the fluoride ions into their structure. Therefore, it is thought that the fluoride ions may play additional roles such as charge balance and acting as templates or structure directing agents.[5] By probing the location of the fluoride ions in zeolite frameworks, it is hoped that significant insight into these additional roles of fluoride ions in zeolite syntheses can be gained and used in a predictive manner.

Despite the importance of the role that fluoride ions play in this synthesis method, there are very limited structural data concerning the location of fluoride ions in purely siliceous zeolite frameworks. Single-crystal XRD, the method of choice for determining structures of crystalline solids, is limited in its application to zeolites due to their microcrystalline nature and to problems arising from crystal twinning.[21] There are additional complications in that fluorine and oxygen have very similar numbers of electrons making them difficult to distinguish. In particular, F^- anions are isoelectronic with the OH groups which can occur as defects within zeolite frameworks. There are only four crystal structures of as-synthesized purely siliceous zeolite materials made via the fluoride route which unambiguously locate the fluoride ions: two single-crystal structures of clathrasil materials and two zeolite structures determined by synchrotron XRD on very small single crystals.

The single-crystal structure of the clathrasil octadecasil[17] revealed a fluoride ion location in a small interstitial cavity of the framework: a double four-ring or $[4^6]$ cage (cages are denoted as $[n^m n'^{m'}...]$ according to the number m of windows consisting of n Si atoms). This location is quite far away from the template cation, demonstrating that the fluoride ions are not found exclusively as intimate ion pairs with the template cation, and hence that their locations may be determined by other effects, perhaps related to templating or structure-directing roles. In the single-crystal structure of another clathrasil nonasil,[18] the fluoride ion is also located a considerable distance away from the template in a small $[4^15^46^2]$ cage of the framework. Furthermore, in this case, the fluoride ion was found to be directly covalently bonded to one of the silicon atoms in the four-ring of this cage, creating a five-coordinate $SiO_{4/2}F^-$ silicon site. This phenomenon of five-coordinate $SiO_{4/2}F^-$ sites in the four-rings of small interstitial cavities of zeolite frameworks has also been observed recently in the crystal structures of zeolite SSZ-23[19] and ITQ-4[20] determined from low-temperature synchrotron XRD data collected on very small crystals. The observation of fluoride ions located in small cages of the framework is not limited to purely siliceous zeolites, as fluoride ions have been found in the frameworks of several $AlPO_4$ and $GaPO_4$ materials synthesized in a similar fashion via the fluoride route.[6] The fluoride ions in these materials have been found to occupy three different types of environments: in the small double four-ring structural units, as a bridging atom between gallium or aluminum atoms, or as a terminal Ga-F group.[6,22]

Although tetrapropylammonium fluoride silicalite-1 ([TPA]-F-[Si-MFI]), an as-synthesized siliceous zeolite with the MFI topology,[23] was the first material synthesized via the fluoride route and one where the improvements in the quality of the crystals due to this synthesis method are most apparent, the location of the fluoride ion within this framework is still unknown. There have been attempts to locate the fluoride ion in [TPA]-F-[Si-MFI]; however, the answer remains ambiguous as there are several proposed locations. In an XRD study of a twinned crystal, Price et al. proposed the fluoride ion to be in the channel intersection, 2.45 Å away from the positively charged nitrogen of the TPA template.[21] Using published atomic coordinates for the MFI framework and TPA cation template,[24] Mentzen et al. constructed Fourier electron density difference maps from powder X-ray diffraction data collected on a [TPA]-F-[Si-MFI] sample and observed two extraframework sites: one in a $[4^15^26^2]$ cage of the framework and the other in the channel intersection, 2.32 Å from the nitrogen of the template cation.[25] Although the site in the framework cage was assigned to the fluoride ion, no satisfactory explanation could be given for the site in the channel intersection. The aim of the present work is to resolve this discrepancy and present an unambiguous location of the fluoride ion in [TPA]-F-[Si-MFI].

Koller et al. showed that the presence of five-coordinate $SiO_{4/2}F^-$ sites in a purely siliceous zeolite could also be detected by solid state $^1H \rightarrow {}^{29}Si$ cross polarization (CP) MAS NMR spectroscopy, as these five-coordinate silicon sites give resonances that are shifted to high field (around -145 ppm) and are substantially enhanced by $^{19}F \rightarrow {}^{29}Si$ cross polarization.[13] In the case of some materials, a broad peak between -115 and -150 ppm appears in the ^{29}Si spectrum due to an exchange process involving the fluoride ions in which they are thought to be mobile between different $SiO_{4/2}$ tetrahedra.[13] This motion gives rise to an average chemical shift for silicon sites whose environments change between four-coordinate $SiO_{4/2}$ and five-coordinate $SiO_{4/2}F^-$. By lowering the temperature, this motion can be "frozen out", yielding a narrow peak at around -145 ppm.[12,13] Thus far, five-coordinate $SiO_{4/2}F^-$ sites have been detected by ^{29}Si CP MAS NMR spectroscopy in some seven structures in total, including [TPA]-F-[Si-MFI].[12]

Although ^{19}F MAS and ^{29}Si CP MAS NMR can detect the presence of fluoride ions and $SiO_{4/2}F^-$ sites, these techniques alone cannot determine the *location* of fluoride ions within zeolite frameworks. Using two-dimensional NMR spectroscopy, it is possible to assign the resonances in the ^{29}Si spectrum to each of the unique silicon sites in a zeolite framework. The two-dimensional INADEQUATE experiment, which probes connectivities between nuclei via the *J*-coupling, has been previously used to successfully assign the peaks in the ^{29}Si spectra of a variety of zeolites.[26−30] Once the peaks are assigned, there are a number of solid-state NMR experiments which can be employed to measure $^{19}F-{}^{29}Si$ distances and therefore locate the fluoride ion. Cross polarization,[31−36] Rotational Echo Double Resonance (REDOR),[37,38] and Transferred Echo Double Reso-

(19) Camblor, M. A.; Díaz-Cabañas, M.-J.; Perez-Pariente, J.; Teat, S. J.; Clegg, W.; Shannon, I. J.; Lightfoot, P.; Wright, P. A.; Morris, R. E. *Angew. Chem., Int. Ed. Engl.* **1998**, *37*, 2122.

(20) Bull, I.; Villaescusa, L. A.; Teat, S. J.; Camblor, M. A.; Wright, P. A.; Lightfoot, P.; Morris, R. E. *J. Am. Chem. Soc.* **2000**, *122*, 7128.

(21) Price, G. D.; Pluth, J. J.; Smith, J. V.; Bennett, J. M.; Patton, R. L. *J. Am. Chem. Soc.* **1982**, *104*, 5971.

(22) Matijasic, A. M.; Paillaud, J. L.; Patarin, J. *J. Mater. Chem.* **2000**, *10*, 1345.

(23) Meier, W. M.; Olson, D. H.; Baerlocher, C. *Atlas of Zeolite Structure Types*, 3rd ed.; Elsevier: New York, 1996.

(24) van Koningsveld, H.; van Bekkum, H.; Jansen, J. C. *Acta Crystallogr.* **1987**, *B43*, 127.

(25) Mentzen, B. F.; Sacerdote-Peronnet, M.; Guth, J. L.; Kessler, H. *C. R. Acad. Sci. Paris, Ser. II* **1991**, *313*, 177.

(26) Fyfe, C. A.; Feng, Y.; Gies, H.; Grondey, H.; Kokotailo, G. T. *J. Am. Chem. Soc.* **1990**, *112*, 3264.

(27) Fyfe, C. A.; Grondey, H.; Feng, Y.; Kokotailo, G. T. *J. Am. Chem. Soc.* **1990**, *112*, 8812.

(28) Fyfe, C. A.; Feng, Y.; Grondey, H.; Kokotailo, G. T.; Mar, A. *J. Phys. Chem.* **1991**, *95*, 3747.

(29) Fyfe, C. A.; Grondey, H.; Feng, Y.; Kokotailo, G. T.; Ernst, S.; Weitkamp, J. *Zeolites* **1992**, *12*, 50.

(30) Morris, R. E.; Weigel, S. J.; Henson, N. J.; Bull, L. M.; Janicke, M. T.; Chmelka, B. F.; Cheetham, A. K. *J. Am. Chem. Soc.* **1994**, *116*, 11849.

(31) Hartmann, S. R.; Hahn, E. L. *Phys. Rev.* **1962**, *128*, 2042.

(32) Pines, A.; Gibby, G.; Waugh, J. S. *J. Chem. Phys.* **1973**, *59*, 569.

nance (TEDOR)[39,40] experiments, which probe the heteronuclear dipolar couplings between nuclei, have been demonstrated to be reliable in measuring distances between isolated $^{19}F/^{29}Si$ spin pairs in octadecasil.[36,41,42]

The aim of the present work is to unambiguously determine the location of the fluoride ion in as-synthesized [TPA]-F-[Si-MFI] zeolite using these solid-state NMR techniques. In structural studies of small molecules or ions occluded in zeolites such as this, solid-state NMR has advantages over XRD in the many cases where large enough single crystals are not available for XRD. If samples of sufficient quality can be synthesized, the solid-state NMR techniques presented in this paper can be extended to any other fluoride-containing zeolite frameworks.

Experimental Section

Sample. The [TPA]-F-[Si-MFI] zeolite was prepared in a fluoride-containing medium by hydrothermal synthesis in a PTFE-lined autoclave for 15 days at 200 °C following the procedure described by Guth et al.[4] The molar composition of the synthesis mixture was 1.0 SiO_2 (Aerosil 130, Degussa), 0.08 tetrapropylammonium bromide (>98%, Fluka), 0.04 ammonium fluoride, and 20 H_2O. The sample was washed with distilled water and dried at 80 °C overnight.

$^1H/^{19}F/^{29}Si$ Triple Frequency Probe. Because this as-synthesized zeolite still contains the TPA template, it was necessary to apply ^1H decoupling during acquisition to obtain high-resolution ^{29}Si NMR spectra. Therefore, an H/F/X triple-resonance probe capable of operating at ^1H, ^{19}F, and ^{29}Si frequencies simultaneously was required to carry out the NMR experiments which probe the interactions between ^{19}F and ^{29}Si. A separate radio frequency channel with matching and tuning capabilities for fluorine was added to a Bruker $^1H/X$ double frequency CP MAS probe. The ^{19}F circuit had its own radio frequency coil which was mounted externally on the cylindrical MAS stator (Doty Scientific, 7 mm Standard Speed). The coil was a modified version of the Alderman-Grant design[43] having its radio frequency field orthogonal to both the inner solenoid coil and the external magnetic field. Although the outer coil is large, it is relatively efficient due to its being part of a single frequency circuit and its radio frequency field being orthogonal to the external magnetic field: 300 W gives a $\pi/2$ pulse length of 6.5 μs. A full description of this design will be published elsewhere.[44]

NMR Spectrometer. Solid-state NMR experiments were performed on a Bruker DMX-400 spectrometer operating at frequencies of 400.13 MHz for ^1H, 376.434 MHz for ^{19}F, and 79.495 MHz for ^{29}Si. The ^{19}F pulses were routed through a Bruker high-power amplifier tuned to the ^{19}F frequency. The ^{29}Si chemical shifts were referenced to tetramethylsilane (TMS) using Q_8M_8 (the cubic octamer $Si_8O_{12}[OSi(CH_3)_3]_8$) as an external secondary reference. The [TPA]-F-[Si-MFI] sample and a small amount of potassium iodide (to measure the spinning rate) were packed into a 7 mm zirconia rotor with Vespel caps. The $^1H\rightarrow^{29}Si$, $^1H\rightarrow^{19}F$, and $^{19}F\rightarrow^{29}Si$ CP match conditions were found on the [TPA]-F-[Si-MFI] sample, rather than by using a model compound.

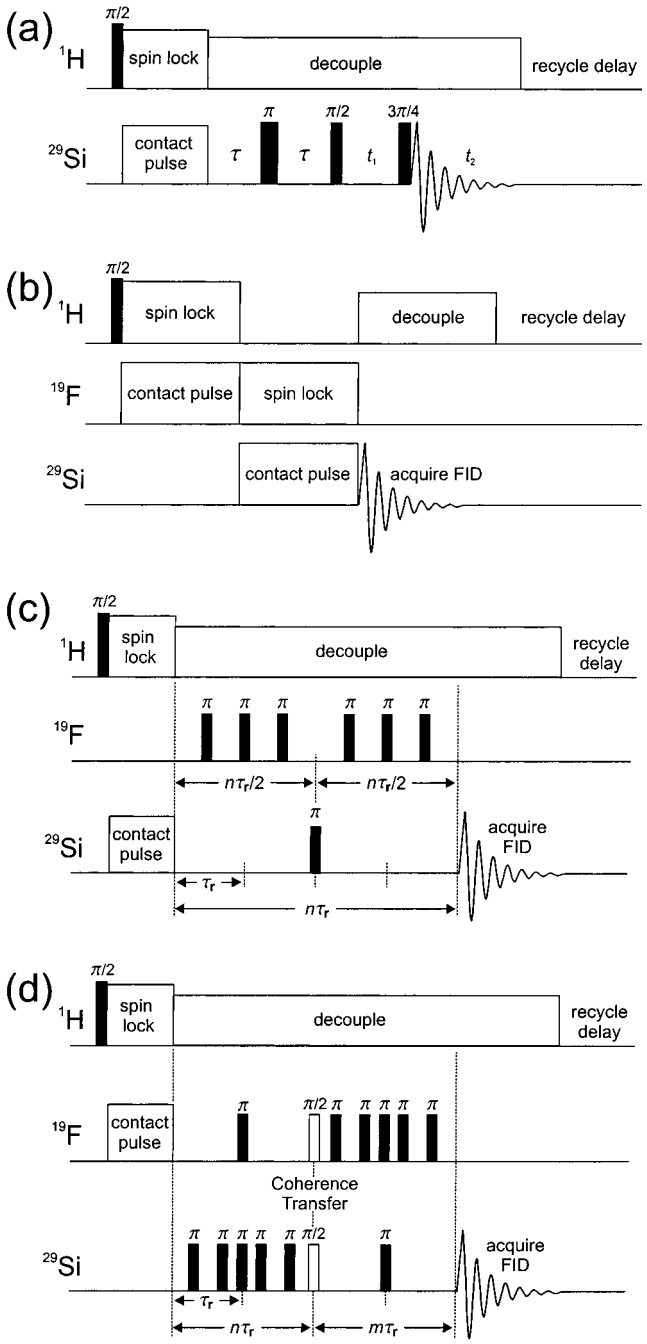

Figure 1. Pulse sequences used: (a) $^1H\rightarrow^{29}Si$ CP-INADEQUATE, (b) $^1H\rightarrow^{19}F\rightarrow^{29}Si$ double cross polarization with ^1H decoupling, (c) $^{19}F/^{29}Si$ REDOR with $^1H\rightarrow^{29}Si$ CP and ^1H decoupling, and (d) $^{19}F/^{29}Si$ TEDOR with $^1H\rightarrow^{19}F$ CP and ^1H decoupling.

All spectra were collected at 327 K, the temperature at which the resonances in the ^{29}Si spectrum are best separated. The following parameters were common to all experiments: 9−11 μs ^1H $\pi/2$ pulse length, 35 kHz ^1H decoupling power, 100 ms acquisition time, and a 2 s recycle delay.

CP-INADEQUATE. The pulse sequence is shown in Figure 1a. The $^1H\rightarrow^{29}Si$ contact time was 10 ms, the ^{29}Si $\pi/2$ and π pulse lengths were 8.0 and 16.0 μs, respectively, and the echo time τ was 8 ms. Sixty-four experiments, each of 1664 scans, were collected in t_1. The sweep widths in the F_1 and F_2 dimensions were 1200 and 2400 Hz, respectively, so that increments in t_1 were synchronized with the 2.4 kHz spinning rate. To increase the resolution, −5 Hz line broadening was applied in the t_2 dimension before Fourier transformation.

Cross Polarization. For $^1H\rightarrow^{29}Si$ CP spectra, 128 scans were collected using a contact time of 10 ms. The spinning rate was 2.0

(33) Stejskal, E. O.; Schaefer, J.; Waugh, J. S. *J. Magn. Reson.* **1977**, *28*, 105.
(34) Mehring, M. *Principles of High-Resolution NMR in Solids*, 2nd ed.; Springer-Verlag: Berlin, 1983.
(35) Hediger, S. *Improvement of Heteronuclear Polarization Transfer in Solid-State NMR*, Ph.D. Dissertation, Eidgenossishe Technische Hochschule, Zurich, Switzerland, 1997.
(36) Fyfe, C. A.; Lewis, A. R.; Chézeau, J. M. *Can. J. Chem.* **1999**, *77*, 1984.
(37) Gullion, T.; Schaefer, J. *J. Magn. Reson.* **1989**, *81*, 196.
(38) Gullion, T.; Schaefer, J. *Adv. Magn. Reson.* **1989**, *13*, 57.
(39) Hing, A. W.; Vega, S.; Schaefer, J. *J. Magn. Reson.* **1992**, *96*, 205.
(40) Hing, A. H.; Vega, S.; Schaefer, J. *J. Magn. Reson. Ser. A* **1993**, *103*, 151.
(41) Fyfe, C. A.; Lewis, A. R.; Chézeau, J. M.; Grondey, H. *J. Am. Chem. Soc.* **1997**, *119*, 12210.
(42) Bertani, P.; Raya, J.; Reinheimer, P.; Gougeon, R.; Delmotte, L.; Hirschinger, J. *Solid State Nucl. Magn. Reson.* **1999**, *13*, 219.
(43) Alderman, D. W.; Grant, D. M. *J. Magn. Reson.* **1979**, *36*, 447.
(44) Fyfe, C. A.; Brouwer, D. H.; Lewis, A. R.; Marcus, T.; Coschizza, M. Manuscript in preparation.

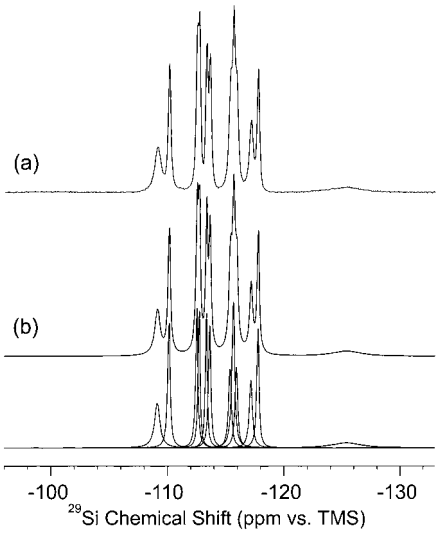

Figure 2. (a) ^{1}H→^{29}Si CP MAS spectrum of [TPA]-F-[Si-MFI], collected at 327 K. (b) Deconvolution of the experimental spectrum with 12 Lorentzian peaks: simulated spectrum (upper) and individual peaks (lower).

kHz. In the ^{1}H→^{19}F→^{29}Si double CP experiment (Figure 1b), 960 scans were collected using a ^{1}H→^{19}F contact time of 12 ms and ^{19}F→^{29}Si contact times between 0.2 ms and 10 ms. The ^{19}F/^{29}Si match condition was set to the −1 spinning sideband of the Hartmann−Hahn match profile and the spinning rate was 3.75 kHz.

REDOR. These experiments consisted of an initial ^{1}H→^{29}Si CP followed by the ^{19}F/^{29}Si REDOR experiment during which ^{1}H decoupling was applied, as shown in the pulse sequence in Figure 1c. At each increment of *n*, two spectra were collected: a reference spectrum in which the dephasing π pulses on ^{19}F are not applied (S_0) and a dephased spectrum in which these dephasing pulses are applied (S_f). The REDOR curve consists of a plot of $\Delta S/S_0$ where $\Delta S = S_0 - S_f$. The ^{1}H→^{29}Si CP contact time was 10 ms, the ^{29}Si π refocusing pulses were 18.8 μs, and the ^{19}F π dephasing pulses were 13.0 μs. The spinning rate was 4.04 kHz. Two-hundred scans were collected for each spectrum.

TEDOR. The pulse sequence is shown in Figure 1d. The contact time for ^{1}H→^{19}F CP was 12 ms. The $\pi/2$ and π pulse lengths for both ^{19}F and ^{29}Si were 6.5 and 13.0 μs, respectively. The number of rotor cycles before coherence transfer (*n*) was incremented while the number of rotor cycles after coherence transfer was fixed at $m = 2$. The dephasing π pulses were applied at 1/4 and 3/4 of the rotor cycles and the refocusing π pulses were applied at $n\tau_r/2$ and $m\tau_r/2$. The spinning rate was 4.01 kHz. 4800 scans were collected for each spectrum. No line broadening or resolution enhancement was applied during processing of the data for the CP, REDOR, and TEDOR experiments.

Calculations. Calculations to deconvolute the ^{29}Si MAS spectra with Lorentzian peaks, to assign the peaks from the results of the INADEQUATE experiment, to fit the oscillations in the CP, REDOR, and TEDOR curves, and to find the location of the fluoride ion were carried out using *Mathematica* version 3.0.[45] Atomic coordinates for the MFI framework used in these calculations were taken from the single-crystal XRD structure of van Koningsveld et al.[24]

Results

The very high quality of this [TPA]-F-[Si-MFI] sample, particularly the lack of Q_3 defects typically found in the products of non-fluoride syntheses, is reflected in the ^{1}H→^{29}Si CP MAS spectrum presented in Figure 2a. The peak widths are sufficiently narrow to resolve all the resonances arising from the crystallographically unique silicon atoms, indicating that the sample is also perfectly ordered on a local basis. At 327 K, the temperature at which the peaks are best separated, the spectrum can be deconvoluted into 12 individual peaks, as shown in Figure 2b, indicating that this material has an orthorhombic *Pnma* structure[21,24] on the NMR time scale. This high resolution of the ^{29}Si spectrum is a critical requirement for the NMR experiments designed to locate the fluoride ion within the framework. However, not all of the peaks are narrow; in comparison to the main group of peaks, the peak at −125 ppm is broadened substantially. Koller et al. proposed that this peak arises from framework silicon sites undergoing dynamic exchange between four- and five-coordinate environments as the fluoride ions are mobile between different $SiO_{4/2}$ tetrahedra.[12,13] The peaks at −109 and −117 ppm in the ^{29}Si spectrum are also broadened slightly, indicating that these silicon sites are also affected by the fluorine exchange process, but to a lesser degree.

To assign the ^{29}Si resonances to each of the unique silicon sites in the MFI framework, a two-dimensional CP-INADEQUATE experiment (Figure 1a) was carried out. When the T_2 relaxation time is long, the optimal echo time τ in the preparation period of the INADEQUATE experiment is $1/(4\boldsymbol{J})$, where $\boldsymbol{J}$ is the scalar *J*-coupling between the coupled nuclei. For the Si−O−Si linkages in zeolites, $\boldsymbol{J}_{Si-Si}$ is thought to be approximately 10 to 15 Hz,[26] which means that ideally τ should be approximately 16 to 25 ms. However, the T_2 values of some of the silicon nuclei in this sample are short: for the broad peak at −125 ppm T_2 is about 6 ms, while T_2 values for the slightly broadened peaks at −109 and −117 ppm are about 40 and 60 ms, respectively, and the T_2 values for the other peaks are greater than 100 ms. Consequently, it was necessary to compromise and use a much shorter echo time of $\tau = 8$ ms, to ensure that not all of the magnetization of these signals dephased during the preparation period. The spectral width was restricted to the group of eleven resolved peaks between −107 and −119 ppm, since as expected, connectivities to the broadest peak at −125 ppm were not observed in experiments with larger spectral widths. The results of this experiment are shown in Figure 3. Nineteen out of twenty-two possible connectivites are observed; no connectivities involving the broadest peak at −125 ppm are seen as expected, and the connectivities to the slightly broadened peak at −109 ppm are very weak at best due to their short T_2 values. Nonetheless, it was possible to assign all the peaks in the ^{29}Si spectrum with those connectivities that were observed. To carry out the analysis, a computer program was written to assign the peaks using the known connectivity pattern of the MFI framework[27] and the connectivites observed in the INADEQUATE experiment. Due to the symmetry of the framework, two equally valid sets of peak assignments are possible, as indicated above the INADEQUATE projection in Figure 3. The correct assignment is indicated in bold; the alternative assignment can be ruled out based on the results of the ^{1}H→^{19}F→^{29}Si double CP experiments described below.

With the peaks assigned to specific silicon sites in the MFI framework, a magnetization transfer experiment from ^{19}F to the ^{29}Si nuclei in the framework will yield direct and unambiguous information about which silicon sites are near the fluoride ion. In the ^{19}F→^{29}Si cross polarization experiment, the rate of the magnetization transfer is expected to depend on the distance between the nuclei: the closer the fluorine ion is to a silicon site, the faster the increase in the ^{29}Si magnetization of that peak. The ^{19}F→^{29}Si CP experiment was performed as a double CP experiment[46−48] in which the magnetization was first transferred

(45) Wolfram, S. *Mathematica: A System for Doing Mathematics by Computer*, Version 3.0; Wolfram Media: Champaign, IL, 1996.

(46) Schaefer, J.; McKay, R. A.; Stejskal, E. O. *J. Magn. Reson.* **1979**, *34*, 443.

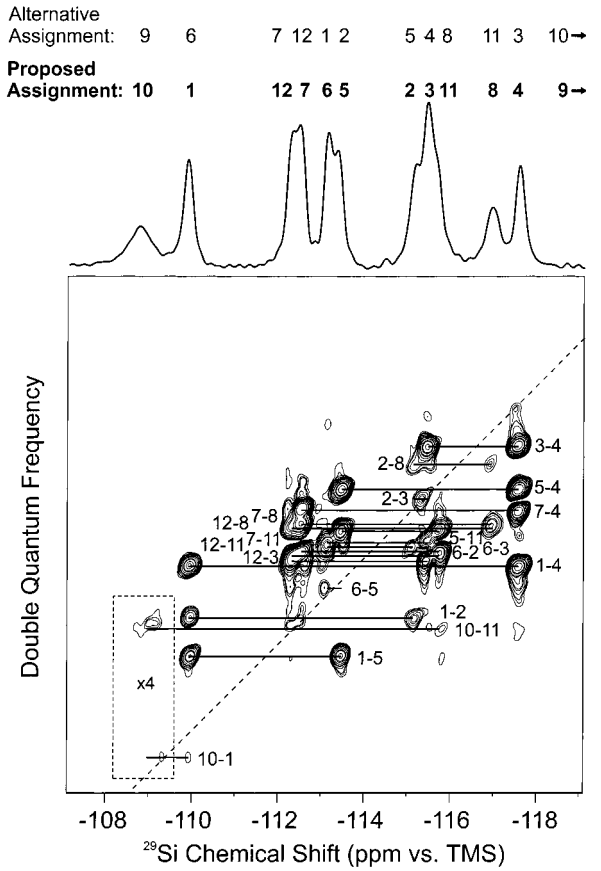

Figure 3. Two-dimensional $^{1}H \rightarrow {}^{29}Si$ CP-INADEQUATE spectrum of [TPA]-F-[Si-MFI] collected at 327 K. Above the 2-D plot is a $^{1}H \rightarrow {}^{29}Si$ CP MAS spectrum with the two possible sets of peak assignments in which the arrows indicate the assignment of the broad peak at −125 ppm. The 19 observed connectivities are labeled according to the proposed assignment scheme (indicated above the projection in boldface text). The alternative assignment can be ruled out by $^{1}H \rightarrow {}^{19}F \rightarrow {}^{29}Si$ double CP experiments (see text).

from ^{1}H to ^{19}F and then from ^{19}F to ^{29}Si. Using an H/F/X triple-resonance probe has two advantages in this situation: ^{1}H decoupling can be used during the acquisition time, without which the ^{29}Si peaks are broadened by interactions with the ^{1}H nuclei to the point where individual resonances are not resolved. An equally important advantage is that T_1 is considerably shorter for the ^{1}H nuclei ($T_1 = 0.7$ s) than for the ^{19}F nuclei ($T_1 = 2.5$ s), which means that the recycle time between experiments can be made much shorter, resulting much better S/N and making variable contact time experiments viable.

In Figure 4, a $^{1}H \rightarrow {}^{19}F \rightarrow {}^{29}Si$ CP MAS spectrum collected with a short contact time is compared to the $^{1}H \rightarrow {}^{29}Si$ CP MAS spectrum. The extreme selectivity of the $^{19}F \rightarrow {}^{29}Si$ transfer clearly shows that the fluoride ion must be closest to silicon sites 8, 9, 10, 11, and 12. These five silicon sites make up a $[4^{1}5^{2}6^{2}]$ cage of the zeolite framework, as shown in Figure 5b. This is very direct evidence that the fluoride ion is located somewhere within this cage and not as an intimate ion pair with the TPA cation template in the channel intersection.

A series of $^{1}H \rightarrow {}^{19}F \rightarrow {}^{29}Si$ CP experiments with contact times between 0.2 and 10 ms were carried out. Using the deconvolution shown in Figure 2, the peak areas for each silicon site

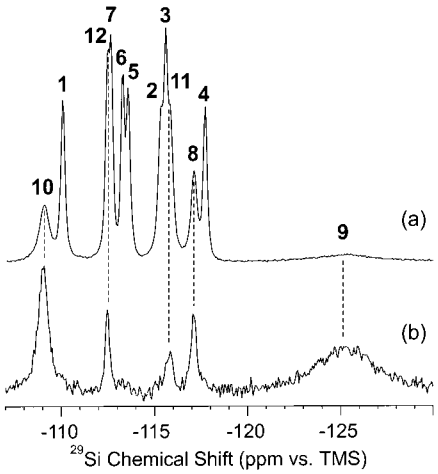

Figure 4. Comparison of (a) the $^{1}H \rightarrow {}^{29}Si$ spectrum to (b) a $^{1}H \rightarrow {}^{19}F \rightarrow {}^{29}Si$ double CP spectrum collected with a short $^{19}F \rightarrow {}^{29}Si$ contact time (0.8 ms) demonstrating the close proximity of silicons 8 through 12 to the fluoride ion.

were extracted from these spectra, yielding the $^{19}F \rightarrow {}^{29}Si$ CP curves shown in Figure 6 which provide further information about the location of the fluoride ion within the $[4^{1}5^{2}6^{2}]$ cage. Comparing the relative rates of magnetization transfer, it is clear that the fluoride ion is closest to Si-9, and the next closest silicon is Si-10, followed by Si-8, Si-12, and Si-11, with Si-1 through Si-7 much further away. A computer program was written to search the MFI unit cell for all positions which have the closest silicon framework sites in the order of Si-9 < Si-10 < Si-8 < Si-12 < Si-11. The possible positions which are in agreement with this order are shown in Figure 5c. The fluoride ion location is now narrowed down to a more specific region within the $[4^{1}5^{2}6^{2}]$ cage.

This same analysis rules out the alternative assignment from the INADEQUATE experiment, as mentioned previously. This alternate assignment has the order of the five closest peaks as Si-10 < Si-9 < Si-11 < Si-7 < Si-8. When the unit cell was searched for possible positions which agreed with this order, no solutions at all were found, indicating that this assignment cannot be correct.

There is another feature in the CP curves that can be exploited to locate the fluoride ion even more specifically. In the CP curves for Si-9, Si-10, and Si-8 there is an oscillatory behavior at the beginning of each curve. This arises from the fact that the ^{19}F and ^{29}Si nuclei are, to a first approximation, isolated spin pairs for those silicons which are close to the fluoride ion. The period of the oscillation depends on the dipolar coupling between the two nuclei, which in turn depends on the distance between them. A sound theoretical analysis of the dynamics of cross polarization between isolated spin pairs in a powder sample under MAS conditions was recently developed by Hediger[35] and summarized in ref 36.

Since the $^{19}F/^{29}Si$ spin pairs are not completely isolated, these CP curves will have contributions from both the isolated spin pairs and the extended network of ^{19}F nuclei. Therefore they were fit to a linear combination of two functions:

$$S_{CP}(t) = M_{CP}[xS_{\text{isolated}}(t) + (1 - x)S_{\text{network}}(t)] \qquad (1)$$

M_{CP} is a scaling factor and S_{network} describes the signal arising from the extended network of ^{19}F nuclei and is described by the exponential growth-decay equation:

(47) Schaefer, J.; Stejskal, E. O.; Garbow, J. R.; McKay, R. A. *J. Magn. Reson.* **1984**, *59*, 150.

(48) Hagaman, E. W.; Ho, P. C.; Brown, L. L.; Schell, F. M.; Woody, M. C. *J. Am. Chem. Soc.* **1990**, *112*, 7445.

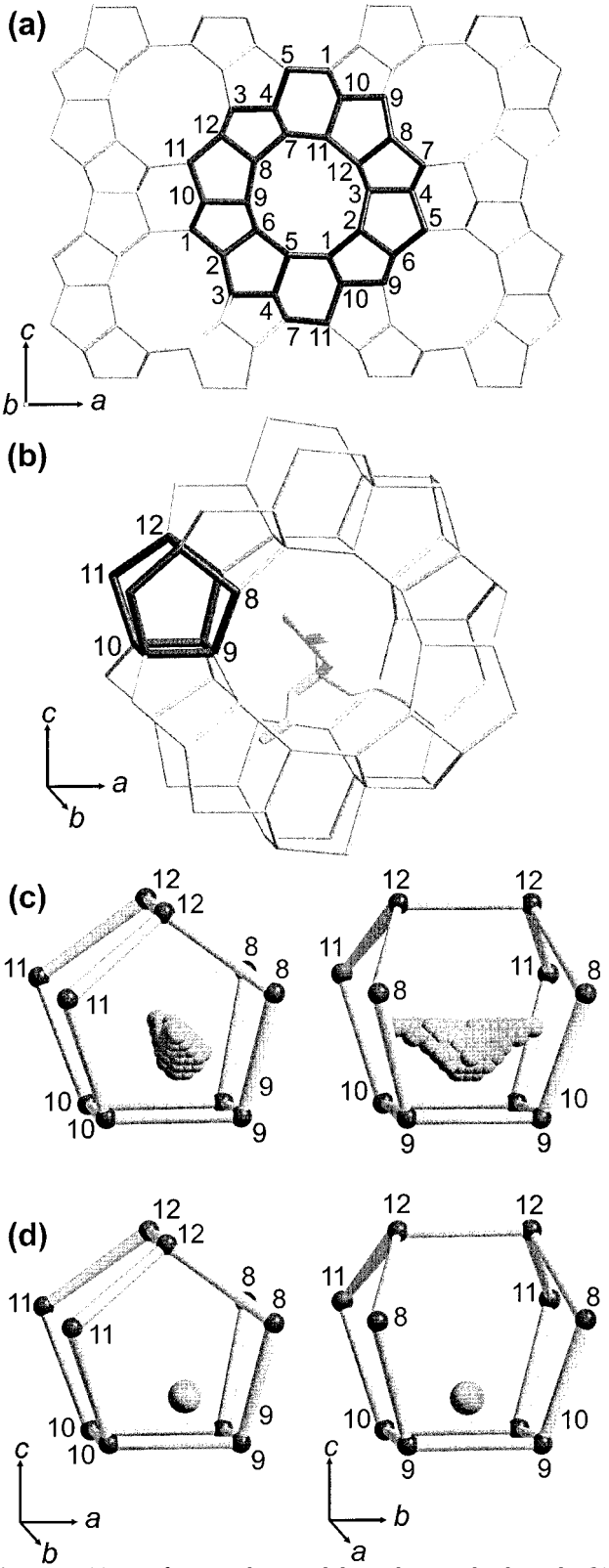

Figure 5. (a) MFI framework viewed down the straight channels. (b) MFI framework around the channel intersection where the TPA cation resides. The [$4^1 5^2 6^2$] cage made up of silicons 8 through 12 is highlighted. (c) Possible fluoride ion locations in the [$4^1 5^2 6^2$] cage which have the closest F−Si distances in the order Si-9 < Si-10 < Si-8 < Si-12 < Si-11 corresponding to the relative rates of magnetization transfer presented in Figure 6. (d) The mean of the fluoride ion locations in the [$4^1 5^2 6^2$] cage which are 2.05 to 2.11 Å from Si-9, 2.65 to 2.75 Å from Si-10, and 3.26 to 3.50 Å from Si-8, according to the fits of the oscillations in the CP curves shown in Figure 8. The location is at fractional coordinates (0.273 ± 0.001, 0.250 ± 0.001, 0.458 ± 0.001).

$$S_{\text{network}}(t) = \frac{\exp(-t/T_{1\rho}) - \exp(-t/T_{CP})}{1 - (T_{CP}/T_{1\rho})} \quad (2)$$

where T_{CP} is the rate constant for the growth of magnetization and $T_{1\rho}$ is the rate constant for magnetization decay due to spin lock relaxation. S_{isolated} is the signal arising from the isolated spin pair and can be described by the equation

$$S_{\text{isolated}}(t) = \frac{1}{2}(\exp(-t/T_{1\rho}) - \exp(-t/T_{\text{damp}})g_{\pm 1}(t)) \quad (3)$$

where T_{damp} is the rate constant for the damping of the oscillation function, $g_{\pm 1}(t)$

$$g_{\pm 1}(t) = \frac{1}{2}\int_0^{\pi} \cos\left(\frac{\pi \boldsymbol{D} t}{\sqrt{2}}\sin(2\theta)\right)\sin\theta \, d\theta \quad (4)$$

$g_{\pm 1}(t)$ is the function derived by Hediger[35] to describe the cross polarization behavior of isolated spin pairs at the ±1 spinning sideband Hartman−Hahn match condition under MAS conditions. Using the methodology developed by Mueller,[49] the integral in eq 4 can be expressed as a sum of Bessel functions of the first kind[36,50]

$$g_{\pm 1}(t) = J_0\left(\frac{\pi \boldsymbol{D} t}{\sqrt{2}}\right) + 2\sum_{k=1}^{\infty} \frac{1}{1 - 4(2k)^2} J_{2k}\left(\frac{\pi \boldsymbol{D} t}{\sqrt{2}}\right) \quad (5)$$

Finally, $\boldsymbol{D}$ is the heteronuclear dipolar coupling constant (in angular frequency units) between the two isolated spin-$^1/_2$ nuclei, which is related to $\boldsymbol{r}$, the distance between the two nuclei:

$$\boldsymbol{D} = (\mu_0 \gamma_I \gamma_S h)/(16\pi^3 \boldsymbol{r}^3) \quad (6)$$

For these equations to be valid, it is necessary to collect CP data at either the +1 or the −1 spinning sideband Hartmann−Hahn match conditions. The Hartmann−Hahn match profile, presented in Figure 7, was constructed by monitoring the intensity of one peak in the ^{29}Si spectrum (Si-10) as a function of the ^{29}Si radio frequency power while keeping the ^{19}F radio frequency power constant. The four maxima are clearly separated by the 3.75 kHz spinning rate. All ^{19}F→^{29}Si CP data presented in this paper were collected at exactly the −1 spinning sideband match condition. It is advantageous to collect CP data at the ±1 match conditions rather than the ±2 match conditions because the S/N is typically higher and the oscillations have a shorter period, leading to reduced uncertainty in the measurement of $\boldsymbol{D}$.

These equations were used to fit the oscillations in the CP curves for Si-9, Si-10, and Si-8 to extract the ^{19}F/^{29}Si dipolar couplings from which F−Si distances can be calculated according to eq 6. The CP curve for Si-9 (Figure 8a) can be fit well with a ^{19}F/^{29}Si dipolar coupling of 2500 ± 100 Hz, corresponding to a F−Si distance of 2.07 ± 0.03 Å. Similarly, fits of the CP curves for Si-10 (Figure 8b) and Si-8 (Figure 8c) yield ^{19}F/^{29}Si dipolar couplings of 1140 ± 60 and 580 ± 60 Hz, which correspond to F−Si distances of 2.70 ± 0.05 and 3.38 ± 0.12 Å, respectively. With these F−Si distances, it is possible to locate the fluoride ion very specifically. A computer program was written to search the solutions presented in Figure 5c for F^- positions which are in agreement with all three observed F−Si distances. The mean and standard deviation of

(49) Mueller, K. T. *J. Magn. Reson. Ser. A* **1995**, *113*, 81.
(50) Vogt, F. G.; Aurentz, D. J.; Mueller, K. T. *Mol. Phys.* **1998**, *95*, 907.

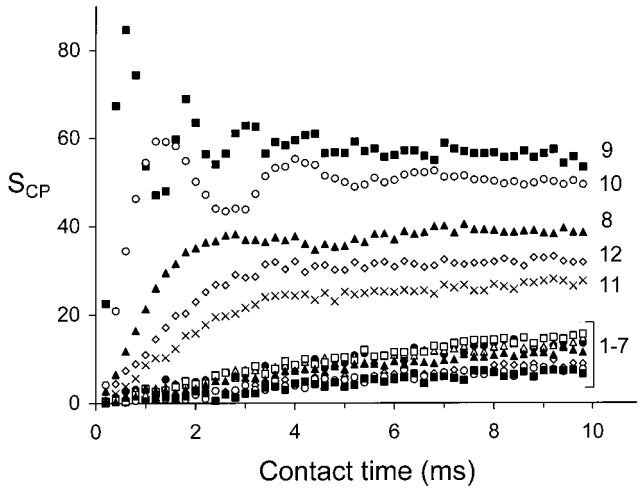

Figure 6. $^{19}F\rightarrow^{29}Si$ CP curves acquired via a $^{1}H\rightarrow^{19}F\rightarrow^{29}Si$ double CP experiment. Peak areas were extracted according to the deconvolution presented in Figure 2.

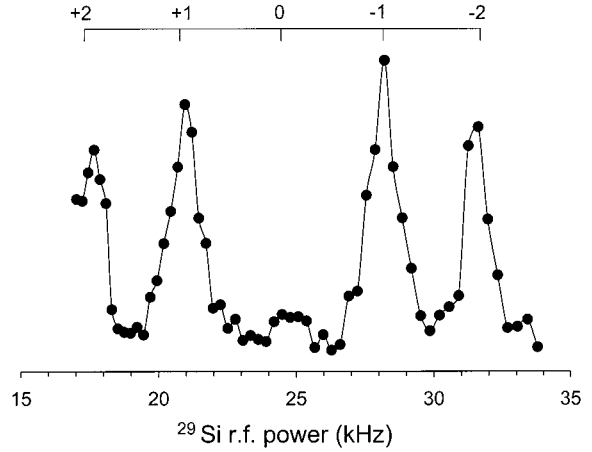

Figure 7. Hartmann−Hahn $^{19}F\rightarrow^{29}Si$ cross polarization matching profile. The intensity of the peak for Si-10 is plotted as a function of the ^{29}Si radio frequency power. The ^{19}F radio frequency power was 24.5 kHz, the spinning rate was 3.75 kHz, and the contact time was 2 ms.

the locations which meet these criteria is at fractional coordinates (0.276 ± 0.001, 0.250 ± 0.001, 0.458 ± 0.001). This location is shown in Figure 5d.

F−Si distances can also be determined by measuring $^{19}F/^{29}Si$ dipolar couplings with REDOR and TEDOR experiments. However, both of these experiments are limited in their ability to measure the closest F−Si distance to Si-9. Both experiments require an accurate measurement of low-intensity signals. Due to the broad nature of the peak for Si-9 arising from motional averaging, it is very difficult to accurately measure the signal among the noise when it is of low intensity. In addition, the success of the REDOR experiment is dependent on T_2 of the ^{29}Si nucleus. In the case of Si-9, the short T_2 leads to a rapid disappearance of the signal, making it even more difficult to get an accurate measurement of the Si-9 signal intensity. Both the REDOR and TEDOR data for Si-9 were not considered reliable enough for distance determination. Nonetheless, it was possible to measure the F−Si distances to Si-10, Si-8, Si-12, and Si-11 by both REDOR and TEDOR.

The results of the REDOR experiment are presented in Figure 9. To determine the $^{19}F/^{29}Si$ dipolar coupling constants from

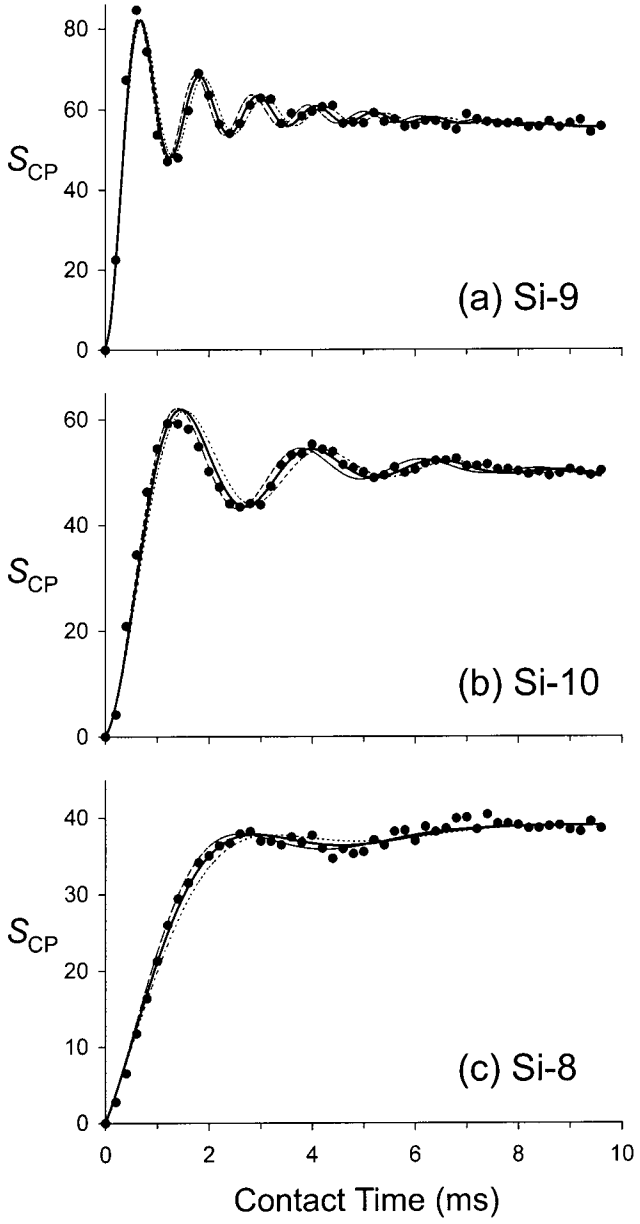

Figure 8. Results of fitting the oscillations in the experimental CP data to theoretical $^{19}F\rightarrow^{29}Si$ CP curves. The best fits are indicated by the solid lines while error estimates are indicated by the dashed lines. (a) Si-9: $\boldsymbol{D} = 2500 \pm 100$ Hz, $M_{CP} = 140$, $x = 0.12$, $T_{damp} = 2.5$ ms, $T_{CP} = 350$ ms, $T_{1\rho} = 95$ ms. (b) Si-10: $\boldsymbol{D} = 1140 \pm 60$ Hz, $M_{CP} = 120$, $x = 0.23$, $T_{damp} = 3.2$ ms, $T_{CP} = 72$ ms, $T_{1\rho} = 29$ ms. (c) Si-8: $\boldsymbol{D} = 580 \pm 60$ Hz, $M_{CP} = 83$, $x = 0.29$, $T_{damp} = 1.9$ ms, $T_{CP} = 8$ ms, $T_{1\rho} = 48$ ms.

which the F−Si distances can be calculated, the REDOR curves were fit with the following function:[49]

$$\Delta S/S_0 = M_R\left(1 - [J_0(\sqrt{2}n\boldsymbol{D}\tau_r)]^2 + 2\sum_{k=1}^{\infty}\frac{1}{16k^2-1}[J_k(\sqrt{2}n\boldsymbol{D}\tau_r)]^2\right) \quad (7)$$

where M_R is a scaling factor that depends on the occupancy of F^- and the efficiency of the experiment, ΔS is the difference between the dephased and reference signal (S_0), n is the number of rotor periods, $\boldsymbol{D}$ is the dipolar coupling constant (see eq 6), and τ_r is the time for one rotor revolution. The $^{19}F/^{29}Si$ dipolar coupling constants and corresponding F−Si distances resulting

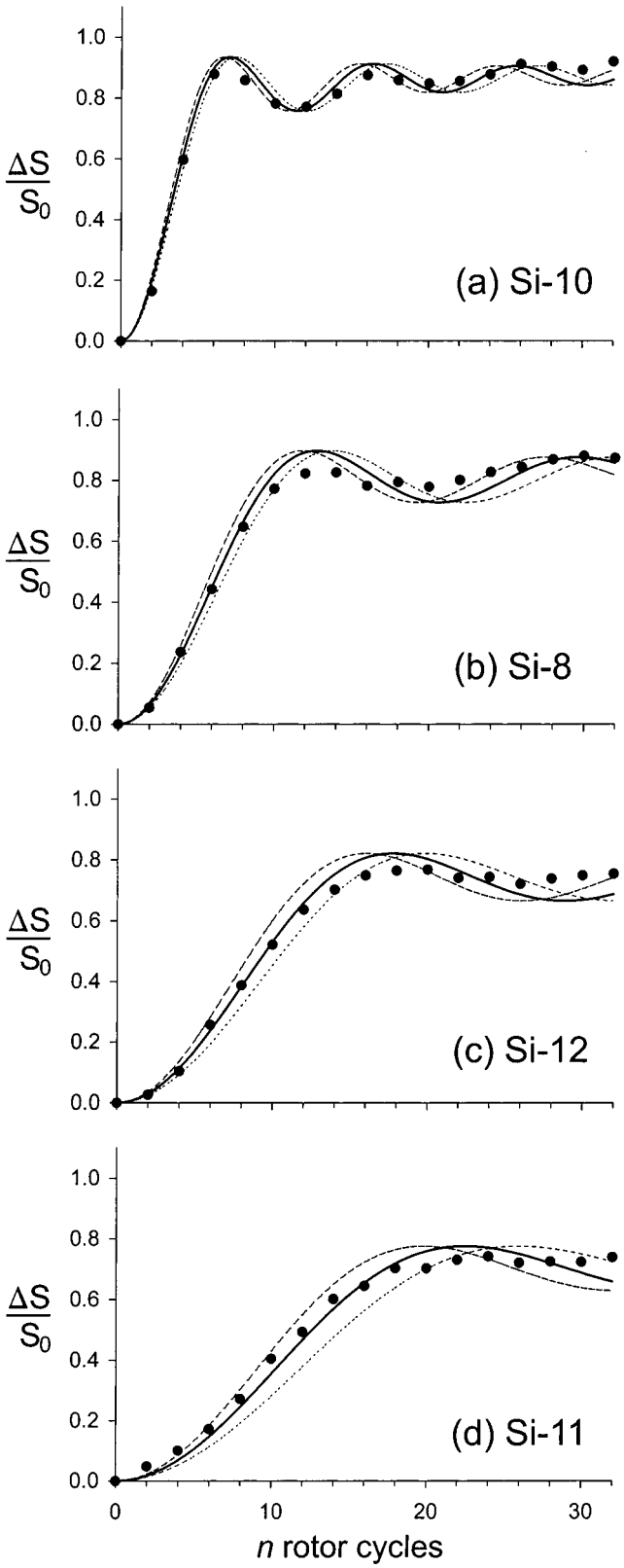

Figure 9. Results of fitting the oscillations in the experimental REDOR data to theoretical $^{19}F/^{29}Si$ REDOR curves. The best fits are indicated by the solid lines while error estimates are indicated by the dashed lines. (a) Si-10: $\boldsymbol{D} = 960 \pm 50$ Hz, $M_R = 0.90$. (b) Si-8: $\boldsymbol{D} = 530 \pm 40$ Hz, $M_R = 0.86$.(c) Si-12: $\boldsymbol{D} = 380 \pm 40$ Hz, $M_R = 0.79$. (d) Si-11: $\boldsymbol{D} = 300 \pm 40$ Hz, $M_R = 0.74$.

from fitting the data with eq 7 are tabulated in Table 1. These distances were then used to locate the F^- at fractional coordinates (0.273 ± 0.001, 0.250 ± 0.001, 0.451 ± 0.001).

Table 1. $^{19}F/^{29}Si$ Dipolar Coupling Constants ($\boldsymbol{D}$) and Corresponding F−Si Distances Determined by CP, REDOR, and TEDOR as Well as Fractional Coordinates of the Fluoride Ion Location Determined from Each Set of Distances

	CP	REDOR	TEDOR
Si-9	2500 ± 100 Hz 2.08 ± 0.03 Å	−	−
Si-10	1140 ± 60 Hz 2.70 ± 0.05 Å	960 ± 50 Hz 2.86 ± 0.05 Å	1000 ± 100 Hz 2.82 ± 0.09 Å
Si-8	580 ± 60 Hz 3.38 ± 0.12 Å	530 ± 40 Hz 3.49 ± 0.09 Å	575 ± 50 Hz 3.39 ± 0.09 Å
Si-12	−	380 ± 40 Hz 3.90 ± 0.14 Å	450 ± 40 Hz 3.68 ± 0.11 Hz
Si-11	−	300 ± 40 Hz 4.21 ± 0.18 Å	360 ± 30 Hz 3.97 ± 0.12 Å
F^- location			
x	0.276 ± 0.001	0.273 ± 0.001	0.286 ± 0.003
y	0.250 ± 0.001	0.250 ± 0.001	0.250 ± 0.002
z	0.458 ± 0.001	0.451 ± 0.001	0.426 ± 0.004

The measured F−Si distances and F^- location are in good agreement with the results of the $^{19}F \rightarrow {}^{29}Si$ CP experiment.

The results of the TEDOR experiment are presented in Figure 10. The equation[49] used to fit the experimental TEDOR curves was

$$S_T = M_T \exp(-n\tau_r/T_{\text{damp}})\left(\frac{1}{2}([J_0(\sqrt{2}(n-m)\boldsymbol{D}\tau_r)]^2 - [J_0(\sqrt{2}(n+m)\boldsymbol{D}\tau_r)]^2) - \sum_{k=1}^{\infty}\frac{1}{16k^2-1}\times ([J_k(\sqrt{2}(n-m)\boldsymbol{D}\tau_r)]^2 - [J_k(\sqrt{2}(n+m)\boldsymbol{D}\tau_r)]^2)\right) \quad (8)$$

where M_T is scaling factor and T_{damp} is a damping factor. By incrementing the number of rotor periods before the coherence transfer (n) and keeping the number of rotor periods after the coherence transfer (m) to a minimum, the experiment was limited by T_2 of the ^{19}F nuclei rather than by T_2 of the ^{29}Si nuclei. However, it was still not possible to accurately measure signal intensities for the broad Si-9 peak due to the low intensity of the signal after the first point. The $^{19}F/^{29}Si$ dipolar coupling constants and corresponding F−Si distances resulting from fitting the data with eq 8 are tabulated in Table 1. Again, these distances were then used to locate the F^- at fractional coordinates (0.286 ± 0.003, 0.250 ± 0.002, 0.426 ± 0.004). The measured distances and location of F^- are in reasonable agreement with the results from both the REDOR and CP experiments.

Discussion

The F−Si distances measured by CP, REDOR, and TEDOR experiments are in good agreement with each other. The distances determined by CP are shorter than the same distances determined by REDOR and TEDOR, a trend that was also observed in measurements on octadecasil.[36,41] REDOR and TEDOR tend to give longer distances as the efficiency of the dipolar dephasing is reduced due to finite pulse lengths, radio frequency inhomogeneity, and instability of the spinning rate; the CP experiment is less affected by these factors.[36] REDOR and TEDOR were not able to accurately measure the F−Si distance to Si-9 due to its short T_2 and broad line width, whereas the CP experiment was not limited by these factors. However, REDOR and TEDOR were more effective in measuring the longer distances to Si-11 and Si-12 as the influence of the

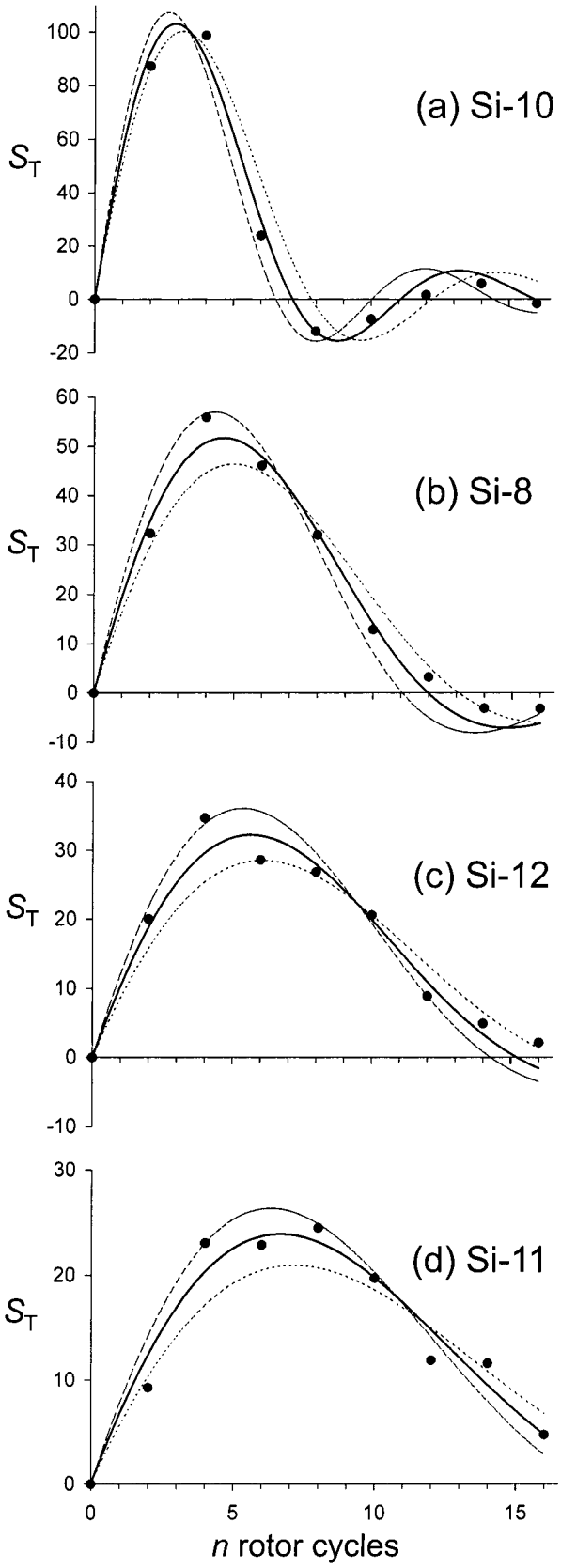

Figure 10. Results of fitting the oscillations in the experimental TEDOR data to theoretical $^{19}F/^{29}Si$ TEDOR curves. The best fits are indicated by the solid lines while error estimates are indicated by the dashed lines. (a) Si-10: $\boldsymbol{D} = 1000 \pm 100$ Hz, $M_T = 300$. (b) Si-8: $\boldsymbol{D} = 575 \pm 50$ Hz, $M_T = 265$. (c) Si-12: $\boldsymbol{D} = 450 \pm 40$ Hz, $M_T = 225$. (d) Si-11: $\boldsymbol{D} = 360 \pm 30$ Hz, $M_T = 220$. All curves had a damping factor of $T_{damp} = 12.5$ ms.

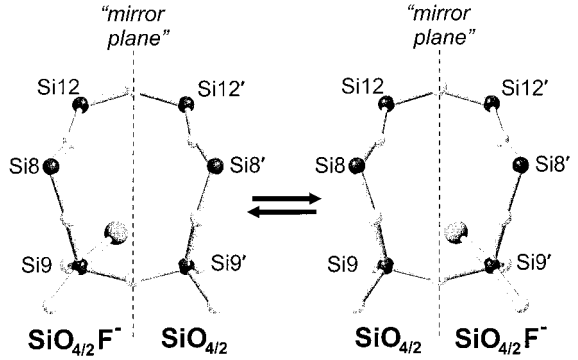

Figure 11. Illustration of the proposed exchange process involving the fluoride ion. The evidence presented in this paper suggests that the fluoride ion jumps between "mirror-related" Si-9 atoms, causing these atoms to exchange between five-coordinate $SiO_{4/2}F^-$ and four-coordinate $SiO_{4/2}$ environments and giving an average structure with orthorhombic *Pnma* symmetry.

extended network of ^{19}F nuclei overwhelmed the oscillations in the CP curves of these nuclei. For all three experiments, the measured F−Si distances could be slightly affected by interactions to distant ^{19}F nuclei, but this effect is difficult to quantify. These experiments show that although each of these techniques measures the heteronuclear dipolar coupling constant, each has its own characteristic advantages and limitations and a more complete structure determination will be obtained when they are used together.

These results shed light onto the nature of the motion of the fluoride ion in [TPA]-F-[Si-MFI]. The INADEQUATE experiment which assigned the broad peak at −125 ppm to Si-9 and the $^1H \rightarrow ^{19}F \rightarrow ^{29}Si$ double CP experiments which demonstrate efficient $^{19}F \rightarrow ^{29}Si$ cross polarization to this site clearly show that Si-9 is the silicon site that is exchanging between four- and five-coordinate environments. The location of the fluoride ion found in this paper is the average position of this exchange process and implies that the fluoride ion motion involves jumping between the "mirror related" Si-9 sites of the framework, as illustrated in Figure 11, making them equivalent on the NMR time scale. We predict that structural analysis at a lower temperature, where this motion is frozen out and the mirror plane is destroyed giving 24 T-sites, will locate the fluoride ion at a position off the mirror plane and directly bonded to Si-9 with a shorter F−Si distance. Since Si-9 is connected to Si-8 and Si-10 (via bridging oxygens), the shorter T_2 values and slight broadening of these peaks which can be seen in the ^{29}Si spectra can also be understood to arise from the fluoride ion motion as the environments around Si-8 and Si-10 change with the dynamics of the Si-9 coordination.

The location of the fluoride ions in [TPA]-F-[Si-MFI] may shed also some light onto the role(s) which they play in the synthesis of this material, particularly the substantial decrease in the number of defects in the crystals. First, the fluorine ions act as the mineralizing agent, facilitating the dissolution of the silica source. Second, the fluoride ions can act as catalysts in the formation of Si−O−Si bonds.[11] The attack of F^- upon the silicon of a four-coordinate SiO_3OH site gives a negatively charged five-coordinate species, which will in turn increase the negative charge on the oxygen atoms around that silicon, favoring nucleophilic attack on a nearby silicon atom which liberates H_2O and, in most cases, F^-. A third possible role of the fluoride ions might be to stabilize Si−O−Si bonds in four-rings. The results presented in this paper and the other XRD structural studies indicate that F^- is most often found near four-rings, often directly bonded to one of the Si atoms which make

up the four-ring. In these cases, one might speculate that the fluoride ion does not act catalytically in assisting the formation of the Si−O−Si linkages, but remains directly bonded to a silicon as these $SiO_{4/2}F^-$ sites in the four-rings may be energetically preferred. This role could be particularly important in the synthesis of [TPA]-F-[Si-MFI] as the four-rings, consisting of Si-9 and Si-10, are formed when pentasil chains are linked together to form sheets. It is possibly in this step of the formation of the MFI framework where incomplete condensation reactions involving the four-rings leads to a large number of defects in non-fluoride syntheses. It is also possible that the fluoride ions could act as structure-directing agents when the sheets link together to form the three-dimensional framework structure. In the case of [TPA]-F-[Si-MFI], the negatively charged $SiO_{4/2}F^-$ sites on one sheet may interact with the positively charged TPA cation template molecules on the surface of another sheet to align and register the sheets to form the MFI framework.

Conclusions

Using the INADEQUATE experiment, it is possible to assign all 12 resonances in the ^{29}Si CP MAS spectrum of [TPA]-F-[Si-MFI] at 327 K. Using this assignment and ^{1}H→^{19}F→^{29}Si double cross polarization experiments, it is possible to locate the fluorine in the [$4^15^26^2$] cage of the zeolite framework. From the oscillations in the CP curves for Si-9, Si-10, and Si-8 it is possible to determine the corresponding F−Si distances, from which the average location of the exchanging fluoride ion can be located. Similarly, experiments with REDOR and TEDOR give F−Si distances to Si-10, Si-8, Si-12, and Si-11 which give the location of the fluoride ion in agreement with the CP experiment. From this location, it is proposed that the fluorine is covalently bonded to Si-9 but jumps between the two "mirror-related" Si-9 sites, making them equivalent on the NMR time scale.

A more complete understanding of the role of fluoride ions in this synthesis method will depend on locating the fluorine in other zeolite frameworks. Undoubtedly, some further structures will be determined by X-ray diffraction, particularly using synchrotron sources, but the general approach outlined here also makes these structures accessible by solid-state NMR. We are currently extending this work to other related systems and are investigating the application of these techniques to the low-temperature structure of [TPA]-F-[Si-MFI] in which the fluorine motion is frozen out.

Acknowledgment. We would like to thank Anne-Catherine Faust for synthesis of the [TPA]-F-[Si-MFI] sample, Tom Marcus and Milan Coschizza for assistance in the design of the H/F/X triple-resonance probe, the Natural Sciences and Engineering Council of Canada for Operating and Equipment grants (C.A.F.) and for the award of a Postgraduate Fellowship (D.H.B.), and the European Commission for the award of a Marie Curie Postdoctoral Fellowship (A.R.L.) (TMR Training Grant Contract No. ERB4001GT974949).

JA010532V